NeuroImage 205 (2020) 116255

Contents lists available at ScienceDirect

NeuroImage

journal homepage: www.elsevier.com/locate/neuroimage

Quantification of apparent axon density and orientation dispersion in the white matter of youth born with congenital heart disease

Kaitlyn Easson [a,b], Charles V. Rohlicek [c], Jean-Christophe Houde [d], Guillaume Gilbert [e], Christine Saint-Martin [f], Kimberly Fontes [a], Annette Majnemer [g,h], Ariane Marelli [i], Pia Wintermark [j], Maxime Descoteaux [d], Marie Brossard-Racine [a,b,h,j,*]

[a] Advances in Brain & Child Development (ABCD) Research Laboratory, Research Institute of the McGill University Health Centre, Montreal, QC, Canada
[b] Department of Neurology & Neurosurgery, Faculty of Medicine, McGill University, Montreal, QC, Canada
[c] Department of Pediatrics, Division of Cardiology, Montreal Children's Hospital, Montreal, QC, Canada
[d] Sherbrooke Connectivity Imaging Laboratory (SCIL), Université de Sherbrooke, Sherbrooke, QC, Canada
[e] MR Clinical Science, Philips Healthcare, Markham, ON, Canada
[f] Department of Medical Imaging, Division of Pediatric Radiology, Montreal Children's Hospital, Montreal, QC, Canada
[g] Department of Pediatrics, Division of Neurology, Montreal Children's Hospital, Montreal, QC, Canada
[h] School of Physical & Occupational Therapy, McGill University, Montreal, QC, Canada
[i] McGill Adult Unit for Congenital Heart Disease, Montreal, QC, Canada
[j] Department of Pediatrics, Division of Neonatology, Montreal Children's Hospital, Montreal, QC, Canada

ARTICLE INFO

Keywords:
Neurite orientation dispersion and density imaging
Diffusion tensor imaging
Congenital heart disease
White matter
Neurodevelopment

ABSTRACT

Background: White matter alterations have previously been demonstrated in adolescents born with congenital heart disease (CHD) using diffusion tensor imaging (DTI). However, due to the non-specific nature of DTI metrics, it is difficult to interpret these findings in terms of their microstructural implications. This study investigated the use of neurite orientation dispersion and density imaging (NODDI), which involves the acquisition of advanced multiple b-value data over two shells and provides proxy measures of apparent axon density and orientation dispersion within white matter, as a complement to classic DTI measures.

Study design: Youth aged 16 to 24 years born with complex CHD and healthy peers underwent brain magnetic resonance imaging. White matter tract volumes and tract-average values of DTI and NODDI metrics were compared between groups. Tract-average DTI and NODDI results were spatially confirmed using tract-based spatial statistics.

Results: There were widespread regions of lower tract-average neurite density index (NDI) in the CHD group as compared to the control group, particularly within long association tracts and in regions of the corpus callosum, accompanied by smaller white matter tract volumes and isolated clusters of lower fractional anisotropy (FA). There were no significant differences in orientation dispersion index (ODI) between groups.

Conclusion: Lower apparent density of axonal packing, but not altered axonal orientation, is a key microstructural factor in the white matter abnormalities observed in youth born with CHD. These impairments in axonal packing may be an enduring consequence of early life brain injury and dysmaturation and may explain some of the long-term neuropsychological difficulties experienced by this at-risk group.

1. Introduction

Brain injury is a frequent neonatal complication of congenital heart disease (CHD), occurring in up to 59% of neonates prior to cardiac surgery (Owen et al., 2011). Specifically, the most common type of brain injury seen in these neonates is white matter injury (Miller et al., 2004), similar to the pattern of injury observed in preterm neonates (Miller et al., 2005). This pattern of diffuse white matter injury presents as a collection of non-cystic, multi-focal lesions on conventional magnetic resonance imaging (MRI), and is associated with the selective death and

* Corresponding author. Advances in Brain and Child Development Research Laboratory Research Institute of the McGill University Health Centre, 5252 boul. de Maisonneuve – 3F.46, Montreal, QC, H4A 3S5, Canada.
E-mail address: marie.brossardracine@mcgill.ca (M. Brossard-Racine).

https://doi.org/10.1016/j.neuroimage.2019.116255
Received 11 July 2019; Received in revised form 10 September 2019; Accepted 7 October 2019
Available online 9 October 2019

arrested maturation of pre-myelinating late oligodendrocyte progenitors (preOLs) (Back and Miller, 2014). With improvements in cardiac surgical techniques and neonatal medical care over the past decades, more than 90% of infants born with CHD now survive beyond the neonatal period and into adolescence and adulthood (Marelli et al., 2016). However, it remains to be determined how neonatal white matter injury evolves into adolescence and adulthood in this population.

Overt white matter abnormalities have been detected on conventional MRI in up to 57% of adolescents born with CHD (Bolduc et al., 2018; Heinrichs et al., 2014; von Rhein et al., 2011). Even in the absence of these overt abnormalities, there may also be subtler alterations to the microstructure of white matter that are below the resolution of conventional MRI. A limited number of studies have examined white matter microstructure in youth born with CHD using diffusion tensor imaging (DTI), which applies information about the diffusion of water molecules through white matter to make indirect inferences about the underlying tissue microstructure. When compared to healthy peers, adolescents born with CHD were found to present with regions of lower fractional anisotropy (FA), suggestive of white matter microstructure alterations, in numerous white matter tracts including the corpus callosum, external capsule, middle cerebellar peduncle, superior longitudinal fasciculus, and uncinate fasciculus (Brewster et al., 2015; Rivkin et al., 2013; Watson et al., 2018). However, FA and other DTI metrics, such as axial diffusivity (AD), mean diffusivity (MD), and radial diffusivity (RD), are inherently non-specific, as they are influenced by several factors related to white matter microstructure such as axon caliber, axon density, axon orientation, and myelination, as well as by free water content (Jones et al., 2013). This hinders the interpretation of these DTI findings, and therefore, it is difficult to form conclusions about the microstructural alterations underlying white matter abnormalities in youth born with CHD.

Neurite orientation dispersion and density imaging (NODDI) (Zhang et al., 2012) is a recently-developed multi-compartment diffusion MRI model that has the potential to provide more specific microstructural insight. In particular, NODDI quantifies tissue microstructure by applying a three-tissue compartment model, including restricted intracellular water, hindered extracellular water, and isotropic free water, to data from a multiple b-value high angular resolution diffusion imaging (HARDI) acquisition. This approach facilitates the extraction of two key metrics that can be referred to as the neurite density index (NDI) and the orientation dispersion index (ODI). NDI is equivalent to the fraction of water contained in the intracellular compartment in each voxel, providing a proxy measure of apparent axon density within white matter. ODI models the degree of dispersion in the orientation of the axons in each white matter voxel. In addition, fitting of the NODDI model allows for the calculation of the isotropic volume fraction (V_{iso}), a measure of free water contamination that provides an avenue to assess the contributions of local edema to alterations in apparent axon density as measured by NDI.

A recent study has applied NODDI to neonates born with CHD as compared to typically developing controls, revealing lower NDI in the bilateral superior frontal occipital fasciculus and posterior limb of the internal capsule and higher ODI in the left corpus callosum, with no differences in V_{iso} in any of the analyzed white matter tracts of interest (Karmacharya et al., 2018). These findings suggest that neonates with CHD display a reduced density of axonal packing in white matter tracts that is not attributable to increased local free water content, with an isolated incidence of increased axonal dispersion. However, this technique has not been used in older individuals born with CHD, which could provide insight regarding the possibly enduring nature of the structural alterations frequently observed in this population.

Therefore, in this study, we used NODDI in conjunction with traditional DTI to compare microstructural organization, particularly as related to the apparent density of axonal packing and coherence of axonal orientation, within white matter tracts between youth born with CHD and healthy controls. As a secondary aim, we also examined the association of observed microstructural alterations with a variety of neuroanatomical and clinical risk factors.

2. Material & methods

2.1. Participants

Term-born youth with complex CHD aged 16 to 24 years who underwent open-heart surgery involving cardiopulmonary bypass before 2 years of age were enrolled in this study. We first recruited participants who participated in a previous study examining developmental outcomes in adolescents born with CHD (Easson et al., 2019). We recruited additional participants from the pediatric and adult cardiology clinics of the McGill University Health Centre.

A control group of healthy, typically-developing youth was recruited through local universities, community flyers, and word of mouth. Control participants were considered typically-developing if they had no history of developmental or neurological conditions and had not received any rehabilitation or special education services during childhood or adolescence. Control participants were matched by age and sex to enrolled CHD participants to produce a control group with a similar age and sex distribution as the CHD group.

Exclusion criteria for both groups included: history of congenital infection, documented chromosomal abnormalities, cerebral palsy, multi-organ dysmorphic conditions, prior history of brain tumour or malformation, documented traumatic brain injury, contraindications for MRI (e.g. confirmed or suspected pregnancy, claustrophobia or vertigo, and ferromagnetic materials, including braces, pacemakers, and cochlear implants), and inability to communicate in English or French. Written informed consent was obtained from participants aged 18 years and older and from the legal guardians of participants younger than 18 years of age. Informed assent was obtained from youth younger than 18 years of age. This study was approved by the Pediatric Research Ethics Board of the McGill University Health Centre.

2.2. Image acquisition

All enrolled participants attended a single study visit involving a brain MRI. Of the 53 youth born with CHD and 48 controls enrolled in this study, 1 participant in the CHD group and 1 participant in the control group opted to not complete the full NODDI acquisition after experiencing discomfort in the MRI machine. The MRI protocol contained a high-resolution anatomical T1-weighted acquisition (TR = 8.1 ms, TE = 3.7 ms, TI = 1010 ms, flip angle = 8°, voxel size = $1.00 \times 1.00 \times 1.00\ mm^3$) and a NODDI acquisition (TR = 9400 ms, TE = 78 ms, flip angle = 90°, voxel size = $2.00 \times 2.04 \times 2.00\ mm^3$) on a 3T MRI System (Achieva X, Philips Healthcare, Best, The Netherlands) using a 32-channel head coil. The NODDI acquisition included a non-diffusion-weighted sequence ($b = 0\ s/mm^2$) with reversed phase encoding and two single-shell HARDI sequences ($b = 700\ s/mm^2$ and 30 directions; $b = 2000\ s/mm^2$ and 60 directions), which each also included a non-diffusion-weighted volume ($b = 0\ s/mm^2$). All images were clinically reviewed for brain abnormalities by an experienced neuroradiologist (C. S. M.), who was blinded to the participants' medical histories. Overt brain abnormalities were subsequently categorized based on their probable origin as either acquired or developmental.

2.3. Image pre-processing

Image processing was accomplished using the TractoFlow pipeline (Theaud et al., 2019), which employs Nextflow (Di Tommaso et al., 2017) and Singularity (Kurtzer et al., 2017). Diffusion-weighted images were denoised using Mrtrix PCA-based denoising (Veraart et al., 2016). Eddy currents and susceptibility and motion artefacts were corrected using Topup and Eddy from FSL, brains were extracted using FSL Bet, and bias field correction was done using ANTs N4 correction (Smith et al., 2004; Tustison et al., 2010). Diffusion-weighted image intensities were

normalized to a common range using Mrtrix, after which the diffusion-weighted images were resampled to the resolution of the T1-weighted images. Pre-processed data from the $b = 700\ s/mm^2$ HARDI sequence were used to compute three-dimensional maps of FA, AD, RD, and MD. Accelerated Microstructure Imaging via Complex Optimization (Daducci et al., 2015) was used to compute three-dimensional maps of NDI, ODI, and V_{iso} using the pre-processed data from the $b = 700\ s/mm^2$ and $b = 2000\ s/mm^2$ HARDI sequences. Fitting the NODDI three-compartment model requires *a priori* values for parallel diffusivity along axons and for isotropic diffusivity in free water. We produced custom estimates of these priors by averaging AD of a cluster of voxels in the corpus callosum and MD in a cluster of voxels in the lateral ventricles, across all subjects. This procedure resulted in a parallel diffusivity prior of approximately $1.64 \times 10^{-3}\ mm^2/s$ (standard deviation $= 7.42 \times 10^{-5}\ mm^2/s$) and isotropic diffusivity prior of approximately $3.34 \times 10^{-3}\ mm^2/s$ (standard deviation $= 1.64 \times 10^{-4}\ mm^2/s$). All raw and pre-processed images, as well as DTI and NODDI metric maps, underwent manual visual quality assessment (K. E.). Participants with persistent artefacts following pre-processing were excluded from statistical analyses. Of the 52 youth born with CHD and 47 controls who

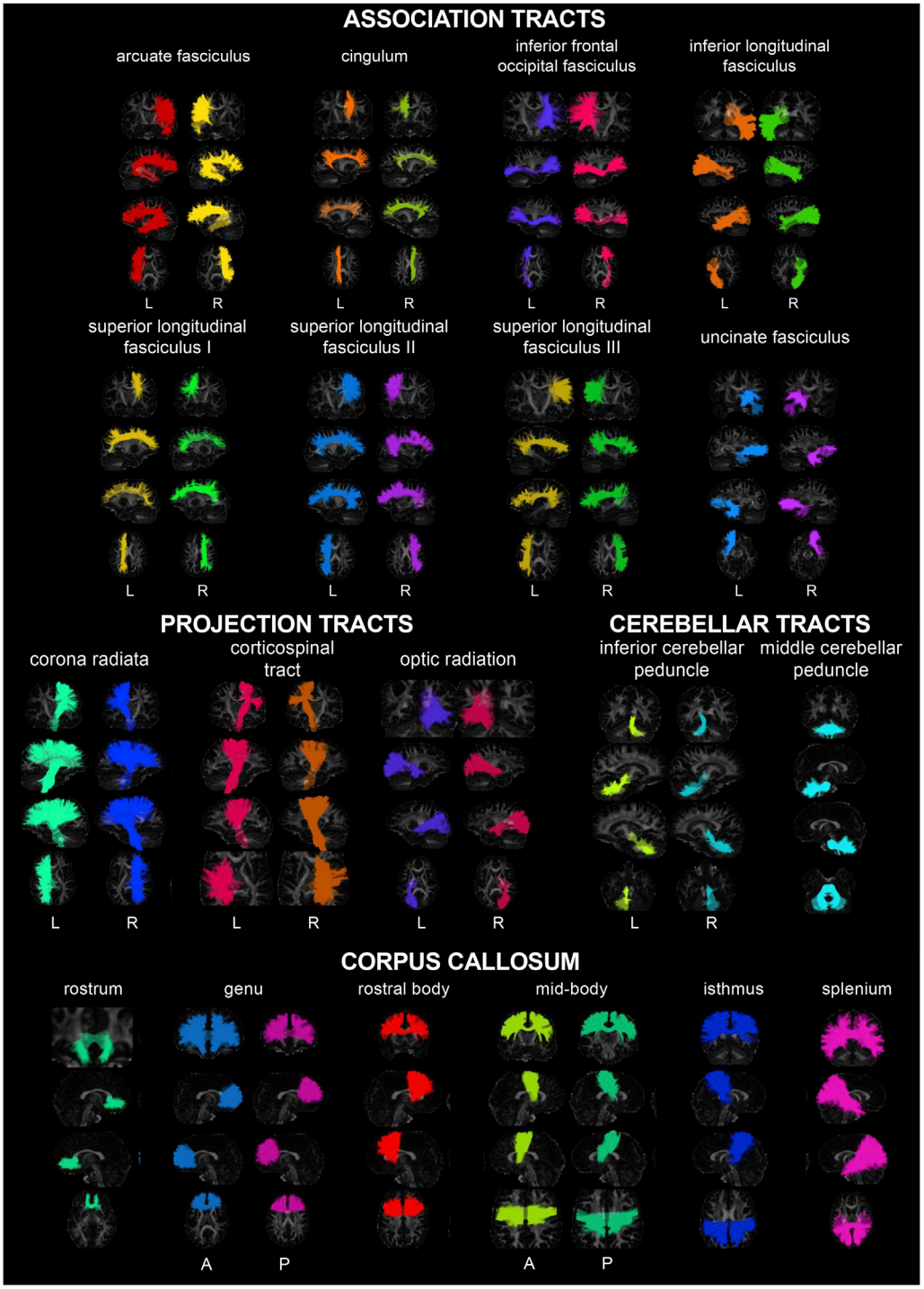

Fig. 1. Extracted white matter tracts of interest.
Legend: L = left, R = right, A = anterior, P = posterior.

completed the NODDI acquisition, data collected from 6 participants in the CHD group and 5 participants from the control group failed visual quality inspection due to artefacts arising from movement during scanning. This resulted in a final sample of 46 youth born with CHD and 42 control youth.

2.4. Tractography and tractometry

Fiber orientation distribution functions were estimated with constrained spherical deconvolution (Tournier et al., 2007). Whole-brain tractograms were generated using probabilistic particle filter tracking (Girard et al., 2014), seeding from the white matter and white matter/-grey matter interface and using 7 seeds per voxel. A modified multi-atlas version of RecoBundles (Garyfallidis et al., 2018) was used to extract 33 bundles that can be categorized into four groups based on their anatomical configuration: association tracts, projection tracts, cerebellar tracts, and eight subdivisions of the corpus callosum (Fig. 1). Of these, the superior longitudinal fasciculus was extracted as four distinct components: the superior longitudinal fasciculus I, the superior longitudinal fasciculus II, the superior longitudinal fasciculus III, and the arcuate fasciculus. These four tracts were extracted separately due to differences in their anatomical pathways and functional specificity (Makris et al., 2005). RecoBundles has been shown to produce robust extraction of white matter bundles, even in the context of incomplete data and pathological brains with structural deformations (Garyfallidis et al., 2018). Tractometry was performed to compute average values of DTI and NODDI metrics for each extracted white matter tract, as well as the volumes of these white matter tracts, for each participant (Cousineau et al., 2017). Each tract underwent visual quality assessment (K. E.) to ensure that each extracted bundle was robust and anatomically accurate. Average DTI and NODDI metric values for tracts that failed this visual inspection for a given participant were excluded from subsequent statistical analyses.

2.5. Individual and clinical characteristics

At the time of the study visit, each participant's weight and height were measured to calculate their body mass index. The Hollingshead Four-Factor Index (Hollingshead, 2011) was used to compute a measure of socioeconomic status for each participant on the basis of parental education and employment. Relevant clinical information was collected from the medical records of the CHD participants, including CHD type, number of open-heart surgeries and cardiac catheterizations, age at first open-heart surgery, bypass and aortic cross clamp duration, use and duration of deep hypothermic circulatory arrest, and use of pre-operative balloon atrial septostomy.

2.6. Statistical analysis

Descriptive statistics were first used to characterize the two groups in terms of individual and clinical characteristics. Shapiro-Wilk tests were used to determine the normality of each continuous demographic variable. Afterwards, independent-samples *t* tests and Mann-Whitney *U* tests were used to compare continuous variables and χ^2 tests and Fisher's exact tests were used to compare categorical variables between groups as appropriate. Comparisons of tract-average DTI and NODDI metric values and white matter tract volumes between the CHD and control groups and between levels of dichotomized risk factors (e.g. presence of overt brain abnormality, type of CHD physiology) were performed using two-sample permutation *t* tests with N = 10 000 permutations. Partial Spearman correlations, controlling for age, were employed to examine the relationship between MRI metrics and white matter tract volumes, given previous evidence of developmental changes in these variables across adolescence and adulthood (Chang et al., 2015; Genc et al., 2017; Lebel and Beaulieu, 2011). For our secondary aim, zero-order Spearman correlations were used to explore associations between MRI metrics and the individual and clinical variables described above. For all analyses, the false discovery rate method was used to correct for multiple comparisons (Benjamini and Hochberg, 1995) and the threshold of statistical significance was considered to be $q < .05$.

2.7. Confirmation with tract-based spatial statistics

To confirm our tract-average results, we additionally performed voxel-wise comparisons of DTI and NODDI metrics between groups using tract-based spatial statistics (TBSS) (Smith et al., 2006) from FSL (Smith et al., 2004). In brief, participants' FA maps first underwent non-linear registration to the FMRIB58_FA template provided with FSL (FMRIB Analysis Group, 2012), after which a mean FA image was calculated and thinned to produce a mean FA skeleton, using an FA threshold of $> .2$. This mean FA skeleton is meant to represent the core white matter of the brain, containing white matter tracts common to all study participants. Each participant's aligned FA, AD, RD, NDI, ODI, and V_{iso} maps were then projected onto this white matter skeleton for voxel-wise statistical analysis. Comparisons of DTI and NODDI metrics between the CHD and control groups were performed with two-sample permutation *t* tests using the FSL randomise tool with N = 10 000 permutations (Nichols and Holmes, 2002). Threshold-free cluster enhancement, fully corrected for multiple comparisons, was used to enhance clusters without selecting an arbitrary cluster threshold (Smith and Nichols, 2009). The threshold of statistical significance was considered to be $p < .05$ (corrected). Significant clusters were identified using the ICBM-DTI-81 white-matter label atlas and the JHU white-matter tractography atlas (Hua et al., 2008; Mori et al., 2005; Wakana et al., 2007).

3. Results

3.1. Participant characteristics

Main individual and clinical characteristics of the final sample (46 youth born with CHD and 42 controls) are outlined in Table 1. Excluded participants did not differ significantly in terms of age, sex, body mass index, or socioeconomic status from included participants.

Table 1
Participants' individual and clinical characteristics.

	CHD (N = 46)	Control (N = 42)	p value
Age (years)	20.0 [16.3–24.1]	20.5 [16.8–24.2]	.187
Sex			.792
Female	25 (54.3%)	24 (57.1%)	
Male	21 (45.7%)	18 (42.9%)	
Body mass index	22.1 [17.3–40.0]	22.7 [19.0–33.8]	.324
Socioeconomic status	40.4 ± 12.4	50.4 ± 10.7	<.001
CHD physiology			
Single-ventricle	10 (21.7%)		
Two-ventricle	36 (78.4%)		
Number of OHS	1 [1–4]		
Number of cardiac catheterizations	1 [0–5]		
Pre-operative BAS	16 (40.0%)		
Age at 1st OHS (days)	33 [0–702]		
Bypass duration, 1st OHS (min)	131 [74–292]		
Aortic cross clamp duration, 1st OHS (min)	75.5 [23–162]		
Use of DHCA, 1st OHS	19 (57.6%)		
DHCA duration, 1st OHS (minutes)	11 [0–52]		

Legend: Descriptive statistics are provided as mean ± SD for normally-distributed continuous variables, median [range] for non-normally-distributed continuous variables, and n (%) for categorical variables. BAS = balloon atrial septostomy, DHCA = deep hypothermic circulatory arrest, OHS = open-heart surgery. Missing variables are excluded from reported percentages (%).

Within the CHD group, 36 participants (78.3%) were born with a two-ventricle cardiac physiology, including dextro-transposition of the great arteries (n = 18), tetralogy of Fallot (n = 11), ventricular septal defect (n = 3), total anomalous pulmonary venous connection (n = 2), and truncus arteriosus type I (n = 2). The remaining 10 participants (21.7%) were born with a single-ventricle cardiac physiology, including double-outlet right ventricle (n = 3), pulmonary atresia with intact ventricular septum (n = 3), double-inlet left ventricle (n = 2), hypoplastic left heart syndrome (n = 1), and Ebstein's pulmonary atresia (n = 1).

3.2. Brain abnormalities on conventional MRI

In our sample, 23.9% (11/46) of youth born with CHD and 11.9% (5/42) of the controls presented with overt brain abnormalities on conventional MRI ($\chi^2 = 2.13$, p = .145). These brain abnormalities are outlined in detail in Table 2. It is important to note that these abnormalities include several mild abnormalities, such as developmental venous anomalies, asymmetrical ventricles, and enlarged perivascular spaces, that may be considered developmental variants rather than truly pathological abnormalities. However, as the cross-sectional design of this study prevents us from ascertaining the true origin of these abnormalities, we have opted to consider these variants as abnormal given the known risk for overt brain abnormalities in the CHD population and their frequency in our sample.

Brain abnormalities likely from an acquired origin were detected in 17.4% (8/46) of youth born with CHD and 9.5% (4/42) of the controls and were more prevalent than abnormalities likely from a developmental origin, which were detected in 15.2% (7/46) of youth born with CHD and 4.8% (2/42) of the controls. Furthermore, 8.7% (4/46) of youth born with CHD and 2.4% (1/42) of control youth presented with multiple (≥2) brain abnormalities (p = .363). Participants with and without overt brain abnormalities did not differ from one another in terms of age, sex, or body mass index.

3.3. Tractometry of DTI and NODDI metrics

Due to failure to pass visual inspection, tract-average DTI and NODDI metric values were excluded for the left and right inferior cerebellar peduncle in 4 CHD and 3 control participants, the left inferior frontal occipital fasciculus in 3 CHD and 7 control participants, the right inferior frontal occipital fasciculus in 3 CHD and 8 control participants, and the rostrum of the corpus callosum, left and right superior longitudinal fasciculus I, and left and right uncinate fasciculus in one CHD participant each.

There were no significant differences between the CHD and control groups in terms of FA, AD, or RD that remained significant after correcting for multiple comparisons. Comparisons of tract-average DTI metrics are outlined in Table 3.

While there were no significant differences in ODI or V_{iso} between the two groups that remained significant after correcting for multiple comparisons, NDI was significantly lower in the CHD group as compared to the control group in the rostral body and anterior and posterior mid-body of the corpus callosum, the right inferior longitudinal fasciculus, and the left and right arcuate fasciculus, cingulum, uncinate fasciculus, and superior longitudinal fasciculus I, II, and III (Fig. 2). Comparisons of tract-average NODDI metrics are outlined in Table 4.

Table 2
Conventional MRI results.

	CHD (N = 46) n (%)	Control (N = 42) n (%)
Normal brain MRI	35 (76.1%)	37 (88.1%)
Abnormalities most likely from a developmental origin		
Grey matter heterotopia	3 (6.52%)	1 (2.38%)
Cortical developmental anomaly	1 (2.17%)	–
Developmental venous anomaly	3 (6.52%)	2 (4.76%)
Chiari I malformation	1 (2.17%)	–
Abnormalities most likely from an acquired origin		
Space occupying lesion	1 (2.17%)	–
Periventricular white matter injury	1 (2.17%)	–
Asymmetrical ventricles	2 (4.35%)	1 (2.38%)
Enlarged perivascular spaces	2 (4.35%)	–
Focal susceptibility artefact	2 (4.35%)	–
Diffuse susceptibility artefact	–	3 (7.14%)

3.4. Voxel-wise confirmation of DTI and NODDI results with TBSS

When confirming our tract-average results using TBSS, the CHD group presented with only a paucity of isolated clusters of lower FA as compared to the control group (Fig. 3A), including clusters in the body of the corpus callosum, fornix, minor fimbria, and left external capsule, and bilaterally in the inferior frontal occipital fasciculus and uncinate fasciculus. There were no clusters in which FA was significantly higher in the CHD group as compared to the controls. Furthermore, there were no clusters in which there were significant differences in AD or RD between groups.

NDI was significantly lower in the CHD group than the control group in many clusters across the mean FA skeleton (Fig. 3B), many overlapping the clusters of significant FA differences. These clusters were found in many white matter regions, including those in which we detected significant tract-average differences in NDI, such as the corpus callosum and bilateral cingulum, superior longitudinal fasciculus, and uncinate fasciculus. Isolated clusters of voxels of significant NDI differences were also found in regions in which we did not detect significant tract-average differences, including the bilateral corona radiata and inferior longitudinal fasciculus. There were no clusters in which NDI was significantly higher in the CHD group as compared to the control group. Additionally, there were no clusters in which there were significant differences in ODI or V_{iso}, in either direction, between the two groups.

3.5. White matter tract volumes

White matter tract volume was significantly smaller in the CHD group as compared to the control group in the right arcuate fasciculus, right cingulum, right inferior longitudinal fasciculus and right superior longitudinal fasciculus III and in the anterior and posterior genu, rostral body, and anterior mid-body of the corpus callosum. Comparisons of white matter tract volumes are outlined in Table 5.

3.6. Contribution of neuroanatomical and clinical variables

When controlling for age, NDI was moderately correlated with white matter tract volume in the posterior genu of the corpus callosum ($\rho = 0.441$, $q = 0.021$) and the left ($\rho = 0.403$, $q = 0.047$) and right ($\rho = 0.467$, $q = 0.021$) superior longitudinal fasciculus I in the CHD group, with no significant correlations in the control group. There were no significant associations between NDI and presence of overt brain abnormalities, socioeconomic status, or body mass index in either group. In the CHD group, neither CHD physiology nor any of the other clinical variables explored were found to be significantly associated with NDI in any of the white matter tracts.

4. Discussion

As the first study of youth born with CHD to employ NODDI, a novel diffusion MRI technique, we revealed widespread reductions in the apparent density of axonal packing in numerous white matter tracts. In contrast, there were no alterations in axonal orientation dispersion within white matter tracts in our sample. These findings suggest that lower density of axonal packing, rather than alterations in axonal alignment, is a predominant microstructural factor contributing to the

Table 3
Comparison of tract-average DTI metrics between groups.

	FA			AD (10^{-3} mm^2/s)			RD (10^{-3} mm^2/s)		
	CHD (mean ± SD)	Control (mean ± SD)	q value	CHD (mean ± SD)	Control (mean ± SD)	q value	CHD (mean ± SD)	Control (mean ± SD)	q value
Association Tracts									
AF (L)	.443 ± .022	.451 ± .022	.230	1.168 ± .031	1.164 ± .023	.819	.576 ± .029	.567 ± .025	.404
AF (R)	.419 ± .024	.423 ± .021	.570	1.141 ± .034	1.142 ± .037	.989	.587 ± .033	.583 ± .029	.773
CG (L)	.509 ± .034	.523 ± .023	.230	1.250 ± .036	1.265 ± .040	.385	.525 ± .038	.514 ± .024	.359
CG (R)	.476 ± .032	.485 ± .021	.286	1.213 ± .033	1.222 ± .048	.604	.550 ± .038	.544 ± .027	.649
IFOF (L)	.508 ± .027	.516 ± .019	.292	1.315 ± .035	1.323 ± .034	.604	.556 ± .033	.550 ± .025	.659
IFOF (R)	.499 ± .027	.508 ± .021	.230	1.301 ± .032	1.310 ± .040	.604	.561 ± .033	.553 ± .028	.535
ILF (L)	.495 ± .025	.503 ± .019	.230	1.325 ± .042	1.328 ± .037	.876	.578 ± .035	.570 ± .028	.535
ILF (R)	.490 ± .028	.494 ± .020	.570	1.302 ± .036	1.306 ± .041	.819	.575 ± .037	.572 ± .030	.802
SLF1 (L)	.470 ± .026	.477 ± .022	.347	1.302 ± .042	1.308 ± .035	.753	.570 ± .035	.562 ± .027	.535
SLF1 (R)	.454 ± .026	.460 ± .023	.442	1.296 ± .037	1.300 ± .037	.847	.568 ± .035	.570 ± .031	.838
SLF2 (L)	.404 ± .026	.405 ± .024	.911	1.192 ± .030	1.194 ± .025	.876	.562 ± .032	.556 ± .022	.649
SLF2 (R)	.409 ± .026	.413 ± .022	.577	1.189 ± .033	1.194 ± .031	.753	.575 ± .032	.572 ± .029	.802
SLF3 (L)	.443 ± .021	.449 ± .020	.338	1.116 ± .026	1.112 ± .020	.753	.593 ± .032	.590 ± .025	.773
SLF3 (R)	.435 ± .026	.440 ± .019	.446	1.124 ± .031	1.126 ± .038	.876	.588 ± .035	.586 ± .030	.838
UF (L)	.456 ± .038	.476 ± .037	.188	1.154 ± .026	1.155 ± .025	.908	.580 ± .030	.576 ± .026	.773
UF (R)	.438 ± .030	.458 ± .033	.165	1.140 ± .031	1.142 ± .041	.876	.582 ± .037	.578 ± .030	.773
Projection Tracts									
CR (L)	.528 ± .019	.532 ± .019	.570	1.275 ± .030	1.271 ± .026	.753	.515 ± .027	.509 ± .023	.535
CR (R)	.528 ± .024	.530 ± .022	.797	1.281 ± .032	1.281 ± .038	.989	.518 ± .031	.516 ± .033	.838
CST (L)	.534 ± .020	.535 ± .019	.908	1.272 ± .032	1.267 ± .028	.753	.506 ± .024	.504 ± .022	.773
CST (R)	.535 ± .022	.532 ± .022	.656	1.280 ± .031	1.271 ± .040	.604	.506 ± .028	.508 ± .033	.838
OR (L)	.496 ± .023	.504 ± .018	.230	1.275 ± .030	1.271 ± .026	.753	.515 ± .027	.509 ± .023	.535
OR (R)	.495 ± .025	.495 ± .024	.940	1.281 ± .032	1.281 ± .038	.989	.518 ± .031	.516 ± .033	.838
Corpus Callosum									
Rostrum	.530 ± .027	.540 ± .021	.230	1.426 ± .050	1.414 ± .049	.604	.556 ± .045	.538 ± .031	.163
Genu (A)	.502 ± .025	.504 ± .016	.813	1.376 ± .044	1.357 ± .046	.385	.565 ± .040	.559 ± .028	.649
Genu (P)	.497 ± .032	.506 ± .020	.230	1.341 ± .040	1.324 ± .046	.385	.563 ± .048	.546 ± .029	.234
Rostral body	.513 ± .029	.524 ± .020	.230	1.346 ± .043	1.331 ± .050	.454	.547 ± .048	.528 ± .033	.163
Mid-body (A)	.547 ± .029	.558 ± .019	.230	1.385 ± .053	1.370 ± .059	.604	.523 ± .054	.502 ± .036	.163
Mid-body (P)	.548 ± .031	.559 ± .019	.230	1.407 ± .052	1.387 ± .052	.385	.533 ± .061	.510 ± .036	.163
Isthmus	.544 ± .028	.556 ± .020	.227	1.421 ± .054	1.406 ± .042	.454	.539 ± .049	.517 ± .029	.163
Splenium	.582 ± .023	.583 ± .019	.908	1.450 ± .056	1.425 ± .039	.385	.499 ± .042	.492 ± .027	.649
Cerebellar Tracts									
ICP (L)	.427 ± .037	.442 ± .043	.230	1.270 ± .097	1.310 ± .108	.385	.627 ± .055	.621 ± .041	.773
ICP (R)	.422 ± .036	.437 ± .048	.230	1.287 ± .101	1.294 ± .118	.876	.639 ± .050	.619 ± .032	.163
MCP	.544 ± .032	.537 ± .026	.442	1.257 ± .059	1.244 ± .052	.604	.487 ± .040	.489 ± .027	.838

Legend: AF = arcuate fasciculus, CG = cingulum, IFOF = inferior frontal occipital fasciculus, ILF = inferior longitudinal fasciculus, SLF = superior longitudinal fasciculus, UF = uncinate fasciculus, CR = corona radiata, CST = corticospinal tract, OR = optic radiation, ICP = inferior cerebellar peduncle, MCP = middle cerebellar peduncle, A = anterior, P = posterior, L = left, R = right. Significant q values at a threshold of $q < .05$ are indicated in bold font.

non-specific white matter alterations previously detected in this population using traditional DTI.

4.1. Reduced apparent axon density in youth born with CHD

We detected only a limited number of clusters of voxels of reduced FA in youth born with CHD, localized to small regions of white matter in the uncinate fasciculus, inferior frontal occipital fasciculus, external capsule, and minor fimbria. However, these differences were not significant at the tract-average level. These findings are indicative of non-specific alterations to white matter microstructure in these small regions and are consistent with a limited number of existing DTI studies in adolescents born with CHD (Brewster et al., 2015; Rivkin et al., 2013; Watson et al., 2018). In contrast with these isolated regions of lower FA, we observed numerous, widespread regions with lower tract-average NDI in the CHD group as compared to the control group, suggestive of apparent impairments in axonal packing within white matter tracts. These findings were confirmed by our TBSS analyses, which demonstrated overlapping regions of voxel-wise NDI reductions. We also detected a few isolated clusters with lower NDI that were not detected in our tract-average analyses. This may be attributable to the small size of these clusters, which were likely not sufficient to drive significant tract-average differences. Our findings are in line with a previously published NODDI study in neonates born with CHD, which reported lower NDI in the left and right superior frontal occipital fasciculus and left posterior limb of the internal capsule (Karmacharya et al., 2018). This suggests that a lower density of axonal packing may persist from the neonatal period into early adulthood in the CHD population. However, longitudinal studies including repeated MRI scans during infancy, childhood, and adolescence are required to confirm this hypothesis.

Previous work has illustrated that NDI increases across the brain from childhood to adulthood (Chang et al., 2015; Genc et al., 2017; Mah et al., 2017). Many of the tracts in which NDI was lower in our CHD sample were long association tracts, which are known to mature later than the cerebellar, commissural, and projection tracts, with a delayed onset of myelination that continues well into adolescence and adulthood (Lebel and Beaulieu, 2011; Zhang et al., 2007). Therefore, our observations of reduced apparent axon density within these late-maturing white matter tracts might reflect further delay in the maturation of these specific tracts, rather than a static deficit in axon density. However, the presence of lower apparent axon density within the earlier-maturing corpus callosum suggests that there might additionally be permanent alterations in axonal packing. Nevertheless, whether these abnormalities are static across the lifespan or still evolving at this age will need to be confirmed.

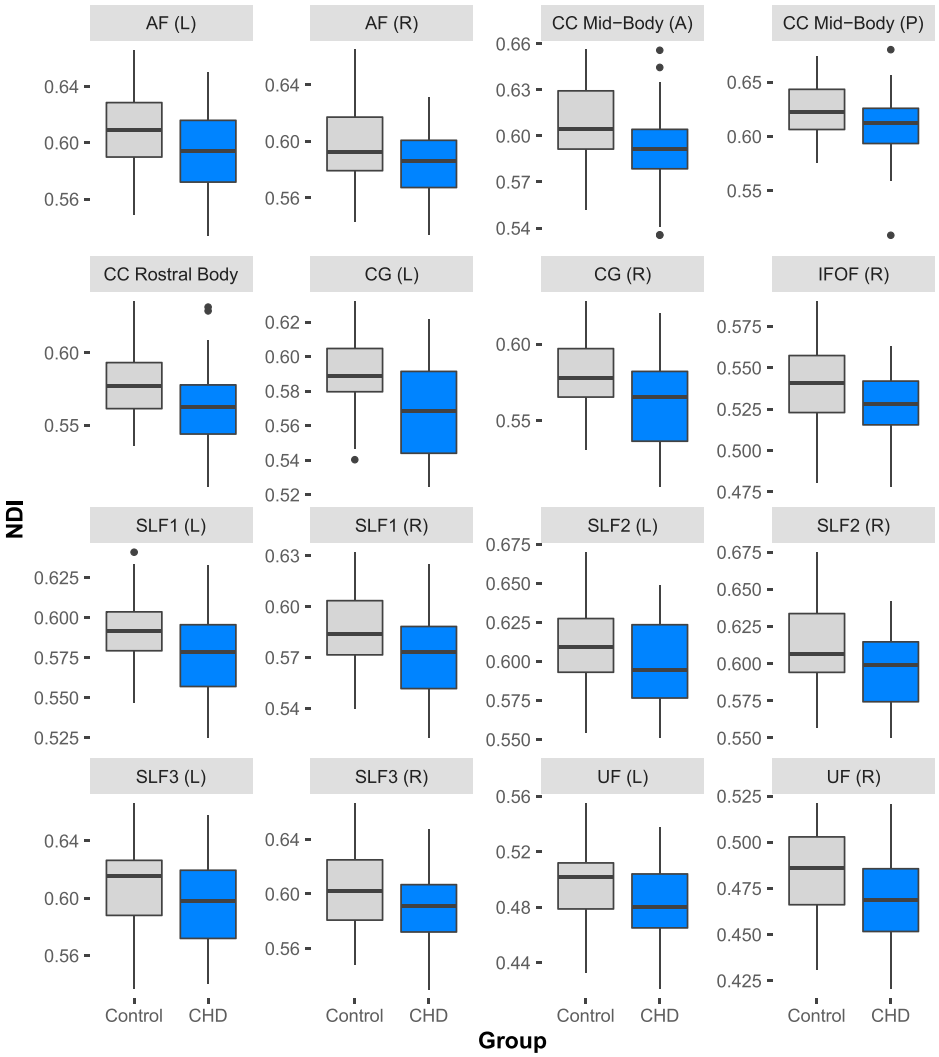

Fig. 2. Significant NDI differences between the CHD and control groups in association tracts and corpus callosum subdivisions.
Legend: AF = arcuate fasciculus, CC = cingulum, CG = cingulum, IFOF = inferior frontal occipital fasciculus, SLF = superior longitudinal fasciculus, UF = uncinate fasciculus, A = anterior, P = posterior, L = left, R = right. All displayed between-groups differences are significant at a threshold of $q < .05$.

Low density of axonal packing in white matter tracts could be the result of either a reduced number of axons through axonal loss or through increased space between axons (Billiet et al., 2014). Insight into the factor responsible for low apparent axon density can be obtained from the proposed mechanism of white matter pathology in the CHD population. In particular, CHD-related white matter injury is thought to arise primarily from hypoxia-ischemia, as a consequence of impaired circulation of oxygenated blood to the fetal and neonatal brain by the structurally-malformed heart (Donofrio et al., 2003). Severe hypoxia-ischemia, presenting in the form of periventricular leukomalacia, results in neuronal death and could contribute to a reduction in axon density, but this pattern of injury is rare in the CHD population. Mild hypoxia-ischemia, which is more probable in the context of CHD, results in the selective death and arrested maturation of particularly vulnerable preOLs (Back and Miller, 2014; Morton et al., 2017), possibly producing long-term deficiencies in myelination. Therefore, impaired myelination of axons in youth born with CHD could result in lower estimates of apparent axon density. In particular, within the NODDI three-compartment model, low myelination would increase the space between axons and estimates of extracellular space, and in turn, drive down estimates of relative intracellular space, and thus NDI. Additionally, mature oligodendrocytes are an important source of trophic factors and metabolic support to axons (Nave, 2010; Simons and Nave, 2015), and as such, interference with the maturation of preOLs to oligodendrocytes could have a detrimental impact on axonal survival, resulting in possible secondary axonal loss and reduced estimates of apparent axon packing density. Additionally, lower estimates of NDI could also be the result of higher local free water content, potentially resulting from inflammation or edema. However, the absence of between-groups differences in V_{iso} rules out the potential contribution of this factor.

Similar to the mechanisms that might underlie reduced density of axonal packing, lower white matter volume, as observed in several white matter tracts in our sample, may also represent axonal loss or deficient myelination. These observations are consistent with previous reports of lower white matter volumes and total brain volumes in youth born with CHD as compared to controls (Fontes et al., 2019; von Rhein et al., 2014). However, significant correlations between white matter volume and axonal packing were restricted to only three white matter tracts in the CHD group, suggesting that microstructural variations in apparent axon density are not directly related to macrostructural alterations in white matter volume. Furthermore, we did not find a significant association between the presence of an overt brain abnormality and NDI, and the observed brain abnormalities in our sample did not spatially overlap with the tracts in which we observed significant between-groups differences in NDI. These findings are in line with previous DTI reports in the CHD population (Rivkin et al., 2013; Watson et al., 2018). This supports the

Table 4
Comparison of tract-average NODDI metrics between groups.

	NDI			ODI			V_{iso}		
	CHD (mean ± SD)	Control (mean ± SD)	q value	CHD (mean ± SD)	Control (mean ± SD)	q value	CHD (mean ± SD)	Control (mean ± SD)	q value
Association Tracts									
AF (L)	.594 ± .028	.609 ± .028	**.035**	.242 ± .012	.241 ± .012	.230	.076 ± .017	.079 ± .018	.575
AF (R)	.584 ± .024	.598 ± .027	**.035**	.257 ± .013	.257 ± .013	.570	.071 ± .018	.076 ± .022	.455
CG (L)	.570 ± .029	.590 ± .023	**.013**	.192 ± .015	.187 ± .013	.230	.055 ± .015	.064 ± .016	.244
CG (R)	.562 ± .030	.581 ± .022	**.023**	.209 ± .014	.206 ± .013	.286	.055 ± .015	.065 ± .020	.247
IFOF (L)	.535 ± .023	.547 ± .029	.089	.177 ± .015	.173 ± .010	.292	.065 ± .018	.069 ± .018	.495
IFOF (R)	.527 ± .022	.540 ± .024	**.035**	.181 ± .012	.176 ± .011	.230	.060 ± .015	.064 ± .018	.495
ILF (L)	.549 ± .030	.561 ± .038	.155	.186 ± .014	.182 ± .009	.230	.085 ± .026	.087 ± .028	.722
ILF (R)	.542 ± .026	.552 ± .032	.155	.191 ± .013	.188 ± .010	.570	.074 ± .021	.078 ± .025	.575
SLF1 (L)	.578 ± .028	.592 ± .022	**.035**	.219 ± .012	.217 ± .011	.347	.064 ± .013	.070 ± .013	.366
SLF1 (R)	.574 ± .026	.587 ± .022	**.035**	.226 ± .013	.223 ± .012	.442	.068 ± .016	.076 ± .020	.366
SLF2 (L)	.597 ± .028	.612 ± .026	**.035**	.272 ± .013	.273 ± .015	.911	.076 ± .017	.081 ± .016	.366
SLF2 (R)	.596 ± .026	.612 ± .027	**.028**	.264 ± .013	.263 ± .013	.577	.075 ± .019	.083 ± .024	.366
SLF3 (L)	.596 ± .030	.610 ± .028	**.045**	.244 ± .008	.242 ± .009	.338	.076 ± .016	.082 ± .016	.366
SLF3 (R)	.589 ± .027	.604 ± .028	**.035**	.249 ± .011	.248 ± .012	.446	.070 ± .019	.077 ± .024	.455
UF (L)	.481 ± .028	.498 ± .027	**.028**	.198 ± .025	.186 ± .024	.188	.035 ± .014	.039 ± .015	.455
UF (R)	.469 ± .027	.484 ± .024	**.028**	.206 ± .017	.195 ± .022	.165	.031 ± .013	.036 ± .017	.366
Projection Tracts									
CR (L)	.644 ± .031	.655 ± .030	.155	.206 ± .014	.205 ± .011	.570	.091 ± .018	.091 ± .014	.822
CR (R)	.637 ± .031	.647 ± .027	.159	.203 ± .014	.202 ± .013	.797	.090 ± .018	.094 ± .022	.495
CST (L)	.653 ± .033	.661 ± .030	.268	.205 ± .013	.205 ± .013	.908	.090 ± .018	.092 ± .015	.635
CST (R)	.648 ± .032	.657 ± .029	.268	.201 ± .013	.205 ± .011	.656	.089 ± .018	.093 ± .024	.575
OR (L)	.576 ± .033	.586 ± .040	.268	.199 ± .014	.193 ± .010	.230	.092 ± .028	.093 ± .028	.822
OR (R)	.569 ± .027	.580 ± .036	.155	.196 ± .013	.194 ± .011	.940	.086 ± .024	.092 ± .027	.495
Corpus Callosum									
Rostrum	.529 ± .036	.533 ± .032	.546	.173 ± .012	.166 ± .012	.230	.082 ± .029	.072 ± .018	.366
Genu (A)	.535 ± .031	.546 ± .031	.155	.187 ± .010	.188 ± .010	.813	.076 ± .022	.074 ± .020	.723
Genu (P)	.542 ± .029	.553 ± .025	.107	.196 ± .013	.193 ± .011	.230	.073 ± .023	.067 ± .019	.455
Rostral body	.562 ± .028	.579 ± .024	**.023**	.191 ± .014	.186 ± .010	.230	.080 ± .027	.076 ± .024	.575
Mid-body (A)	.590 ± .027	.608 ± .026	**.023**	.179 ± .017	.173 ± .011	.230	.093 ± .033	.088 ± .027	.575
Mid-body (P)	.609 ± .029	.624 ± .024	**.035**	.184 ± .022	.175 ± .011	.230	.113 ± .035	.104 ± .026	.455
Isthmus	.600 ± .029	.608 ± .027	.268	.177 ± .016	.167 ± .011	.227	.108 ± .032	.098 ± .022	.366
Splenium	.617 ± .031	.624 ± .037	.330	.157 ± .012	.155 ± .009	.908	.099 ± .031	.095 ± .024	.575
Cerebellar Tracts									
ICP (L)	.634 ± .057	.642 ± .054	.513	.287 ± .029	.269 ± .033	.230	.146 ± .041	.152 ± .035	.612
ICP (R)	.638 ± .057	.646 ± .047	.519	.285 ± .027	.269 ± .040	.230	.153 ± .037	.149 ± .032	.635
MCP	.728 ± .047	.740 ± .045	.270	.219 ± .023	.221 ± .021	.442	.110 ± .027	.113 ± .022	.658

Legend: AF = arcuate fasciculus, CG = cingulum, IFOF = inferior frontal occipital fasciculus, ILF = inferior longitudinal fasciculus, SLF = superior longitudinal fasciculus, UF = uncinate fasciculus, CR = corona radiata, CST = corticospinal tract, OR = optic radiation, ICP = inferior cerebellar peduncle, MCP = middle cerebellar peduncle, A = anterior, P = posterior, L = left, R = right. Significant q values at a threshold of $q < .05$ are indicated in bold font.

importance of using quantitative diffusion MRI approaches to evaluate white matter microstructure, as many microstructural abnormalities are below the level of resolution of the human eye and may be missed on conventional MRI.

Within our sample, NDI was not significantly associated with any of the analyzed individual or clinical risk factors. The lack of an association between NDI and socioeconomic status in our sample falls within a mixed body of literature, with previous findings of both significant and non-significant associations of socioeconomic status with white matter volume and microstructure (Jednorog et al., 2012; Noble et al., 2012; Ursache et al., 2016). The lack of agreement in the existing literature may arise from differences in the clinical features of the study samples or in the scales used to quantify socioeconomic status. Nevertheless, our findings are consistent with a previous DTI study of healthy children that used the Hollingshead Two-Factor index and who also did not find an association between DTI metrics and socioeconomic status (Jednorog et al., 2012).

It is also important to note that there are additional perinatal clinical factors that may be associated with low density of axonal packing. As our sample was born in the 1990s and early 2000s, before the digitalization of medical records, we were limited in our ability to consistently extract additional risk factors for brain injury, such as timing of diagnosis (Peyvandi et al., 2016), pre-operative cardiac arrest (Dimitropoulos et al., 2013), and post-operative blood pressure (McQuillen et al., 2007). Furthermore, our participants were born before the development of technological advancements that now allow us to measure advanced clinical factors such as cerebral oxygenation, which has been shown to be related to brain development in fetuses with CHD (Sun et al., 2015). Together, these limitations prevented us from robustly examining the effects of all possible clinical risk factors.

4.2. Conserved axonal alignment in youth born with CHD

We found no differences in white matter ODI between the CHD group and the control group, on either a voxel-wise basis or a tract-average basis. This is in contrast with a previous study of neonates born with CHD, which detected higher ODI in the left corpus callosum only (Karmacharya et al., 2018). Taken together with our findings, this could suggest that while there may be minor disruptions in the coherent organization of axons in the corpus callosum during infancy in patients born with CHD, these abnormalities may resolve by adolescence. However, without longitudinal studies involving serial MRI scans of the same participants, this interpretation remains speculative.

Previous NODDI studies in typically-developing individuals have

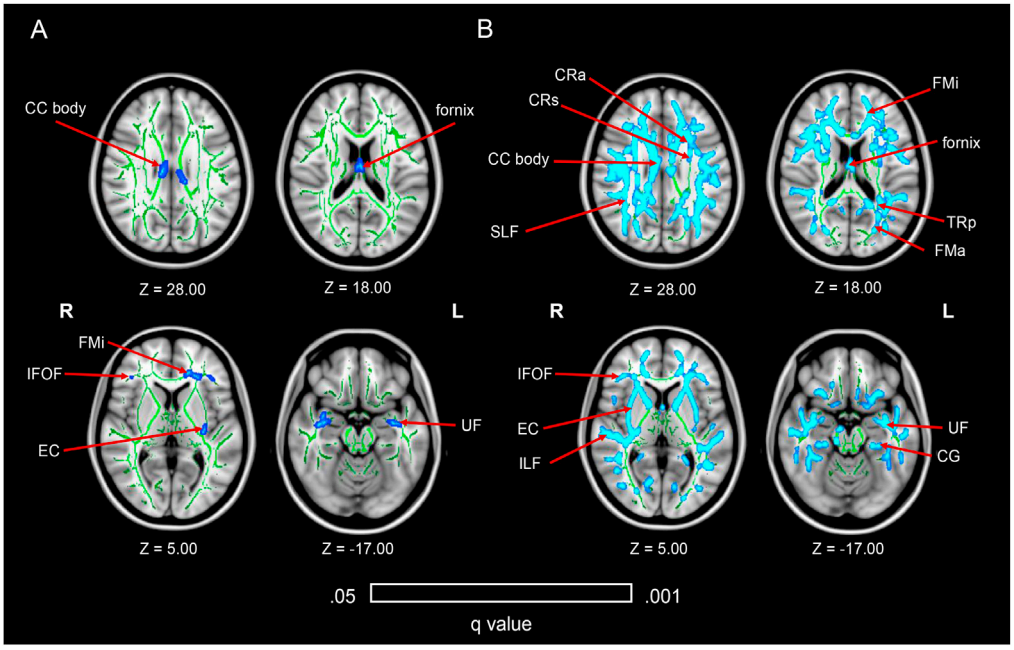

Fig. 3. (A) FA differences between CHD and control groups. (B) NDI differences between CHD and control groups. Blue-light blue colour represents voxels where metric is significantly lower in the CHD group than the control group ($p < .05$, corrected). Mean FA skeleton (green) is overlaid on the MNI152 T1 template. *Legend:* CC = corpus callosum; CG = cingulum; CRa = anterior corona radiata; CRs = superior corona radiata; EC = external capsule; FMa = major fimbria; FMi = minor fimbria; IFOF = inferior frontal occipital fasciculus; ILF = inferior longitudinal fasciculus; SLF = superior longitudinal fasciculus; TRp = posterior thalamic radiation; UF = uncinate fasciculus; L = left; R = right.

suggested that axonal alignment, as measured by ODI, has a greater influence on FA than apparent axon density, as measured by NDI (Zhang et al., 2012; Mah et al., 2017). The lack of between-groups differences in ODI in our sample coupled with the predominant contribution of ODI to FA over NDI may play a role in the scant FA differences observed between the CHD and control groups. In turn, this suggests the possibility that previous studies of white matter alterations using DTI in the CHD population have in fact under-detected the true extent of white matter dysmaturation in patients with CHD across the lifespan due to the complex, multi-factorial nature of FA. This highlights the benefit of employing novel quantitative MRI techniques to detect not only the true microstructural nature, but also the true severity and spatial extent of white matter pathologies in various clinical populations, in the context of the inherent lack of specificity of FA and other DTI metrics.

4.3. Clinical implications of impaired axonal packing

Overall, up to 60% of CHD survivors present with a constellation of neurodevelopmental deficits throughout adolescence and young adulthood, including cognitive difficulties, such as lower intelligence, executive functioning deficits, visual spatial impairments, and reduced academic achievement, accompanied by fine and gross motor impairments, behavioural problems, and a variety of functional limitations (Easson et al., 2019; Abda et al., 2019; Bellinger et al., 2011; Latal, 2016). Given the critical role of white matter tracts in facilitating efficient communication between discrete grey matter regions with different functions, the reductions in apparent axonal packing within white matter tracts observed in our CHD sample may contribute to some of these neurodevelopmental difficulties.

In particular, the majority of white matter tracts in which reduced apparent axon density was observed in the present study were long association tracts, which have been implicated in a variety of higher-order cognitive functions, including language, learning and memory, attention, and visual spatial processing, with an additional role for the cingulum and uncinate fasciculus in emotional processing (Schmahmann et al., 2008). In addition, we observed reduced apparent axon density in the corpus callosum, which has been linked to functions such as reasoning, perception, attention, language, and memory (Schmahmann et al., 2008). Therefore, reduced apparent axon density in these white matter tracts could underlie some of the neurodevelopmental difficulties observed in youth born with CHD. Future structure-function studies are required to explore the potential role of NDI as a precise neural correlate of neuropsychological difficulties in this at-risk group.

4.4. Limitations

The findings of our study should be interpreted in the context of some limitations. First, NODDI is only able to model a single fibre population in each voxel, which is problematic in the context of a previous estimate that up to 90% of white matter voxels contain crossing fibre configurations (Jeurissen et al., 2013). Therefore, future studies in this population could employ modelling techniques that are robust to crossing fibres, such as NODDI-spherical harmonics (NODDI-SH), which incorporates the calculation of fibre orientation distribution functions to allow for accurate estimation of apparent axon density and orientation in voxels with crossing and fanning fibre orientations (Zucchelli et al., 2017). Other alternatives include the spherical mean technique (Kaden et al., 2016) or spherical deconvolution approaches (Dell'Acqua et al., 2013; Raffelt et al., 2012). The field of microstructure modelling has not yet found consensus on the optimal acquisition and modelling scheme to estimate apparent axon density (Lampinen et al., 2019). Another limitation of NODDI is the requirement for *a priori* fixed estimates of parallel and perpendicular diffusivity across the brain. However, these diffusivity values may differ between different regions of the brain and between typically- and atypically-developing brains (Lampinen et al., 2017), which may impede accurate fitting of the NODDI model in all voxels. Finally, NODDI is only able to provide proxy measures of apparent axon density and orientation, and as such, our indirect evidence of reductions in apparent axon density could only be directly confirmed with post-mortem histological studies.

In addition, while RecoBundles has been previously shown to produce robust bundle extraction, we encountered difficulties in the extraction of a small number of tracts, particularly the inferior cerebellar peduncle, possibly due to residual noise in the brainstem, and the inferior frontal occipital fasciculus, possibly due to failed streamline propagation as the bundle funnels through the external capsule. To address this, we excluded DTI and NODDI metric values for tracts that failed to be accurately extracted for a given participant to maintain the integrity of our findings. However, this may have limited the statistical power of the between-groups comparisons for these particular bundles.

Table 5
Comparison of white matter tract volumes (mm^3) between groups.

	CHD (mean ± SD)	Control (mean ± SD)	q value
Association Tracts			
AF (L)	69733 ± 9194	74101 ± 8262	0.057
AF (R)	62020 ± 8645	67544 ± 9225	**0.026**
CG (L)	22933 ± 5906	24677 ± 4991	0.216
CG (R)	20697 ± 5317	25446 ± 5635	**0.007**
IFOF (L)	25416 ± 10263	22006 ± 11749	0.216
IFOF (R)	26486 ± 10300	25577 ± 13529	0.784
ILF (L)	59570 ± 5428	62619 ± 7230	0.084
ILF (R)	56028 ± 5638	59864 ± 6068	**0.025**
SLF1 (L)	24157 ± 7855	25417 ± 8687	0.569
SLF1 (R)	24186 ± 8555	28596 ± 7661	0.055
SLF2 (L)	51793 ± 9827	55720 ± 9926	0.126
SLF2 (R)	48098 ± 8109	48899 ± 8355	0.730
SLF3 (L)	28066 ± 6256	30702 ± 7997	0.159
SLF3 (R)	43295 ± 7720	48038 ± 7239	**0.026**
UF (L)	12935 ± 5196	10977 ± 5794	0.178
UF (R)	15566 ± 5433	14600 ± 6101	0.536
Projection Tracts			
CR (L)	72828 ± 7870	74946 ± 8449	0.294
CR (R)	63428 ± 9508	63966 ± 11578	0.829
CST (L)	48238 ± 6160	46633 ± 11156	0.506
CST (R)	50472 ± 5297	51039 ± 6268	0.730
OR (L)	39686 ± 4587	41052 ± 4464	0.229
OR (R)	37350 ± 4291	39308 ± 3318	0.057
Corpus Callosum			
Rostrum	18790 ± 4617	20538 ± 3982	0.125
Genu (A)	48941 ± 7098	53966 ± 5491	**0.011**
Genu (P)	44261 ± 8100	48908 ± 6042	**0.025**
Rostral body	48158 ± 7681	54130 ± 5775	**0.007**
Mid-body (A)	40433 ± 5142	43873 ± 6349	**0.026**
Mid-body (P)	44408 ± 7776	46650 ± 7689	0.237
Isthmus	52667 ± 10645	56548 ± 10333	0.150
Splenium	102429 ± 17504	109863 ± 16173	0.100
Cerebellar Tracts			
ICP (L)	10481 ± 3918	8725 ± 4158	0.101
ICP (R)	9955 ± 4000	8175 ± 4114	0.101
MCP	23419 ± 6988	23507 ± 6290	0.950

Legend: AF = arcuate fasciculus, CG = cingulum, IFOF = inferior frontal occipital fasciculus, ILF = inferior longitudinal fasciculus, SLF = superior longitudinal fasciculus, UF = uncinate fasciculus, CR = corona radiata, CST = corticospinal tract, OR = optic radiation, ICP = inferior cerebellar peduncle, MCP = middle cerebellar peduncle, A = anterior, P = posterior. Significant q values at a threshold of $q < .05$ are formatted in bold font.

Furthermore, our study included a heterogeneous sample of CHD diagnoses including both single- and two-ventricle cardiac physiologies. While this may prevent our results from being generalizable to a specific CHD subtype, our diverse sample is representative of the CHD population as a whole. Finally, it is also possible that recent advances in cardiac surgical techniques and perinatal care over the past decades, which have not been captured in our cohort, may attenuate some of the white matter abnormalities we observed in this study.

4.5. Conclusion

This study has demonstrated widespread reductions in apparent axon density as measured by NDI in many white matter tracts, particularly long association tracts, in youth born with CHD as compared to healthy controls. These NDI reductions were largely independent of overt brain abnormalities and reduced white matter volume and were accompanied by relatively preserved axonal organization as measured by ODI. Our findings demonstrate the potential of NDI as a more precise and clinically meaningful metric of altered white matter microstructure in CHD as compared to FA and highlight the importance of utilizing more specific MRI approaches to gain precise insight into the mechanisms underlying these commonly-reported microstructural alterations. Given the important role of the corpus callosum and long association tracts in various higher-order cognitive and behavioural functions, these observations of reduced apparent axon density may underlie some of the persistent neuropsychological difficulties experienced by youth born with CHD. Future structure-function studies should aim to confirm the functional consequences of these microstructural white matter alterations in order to gain greater insight into the etiology of the persistent neurodevelopmental challenges faced by youth born with CHD.

Declaration of competing interest

J. C. H. and M. D. are employees of Imeka Solutions Inc. G. G. is an employee of Philips Healthcare.

Acknowledgements

First and foremost, we would like to thank the participants and their families for their participation in this study. We would also like to thank the MRI technologists, research coordinators, and research assistants at the ABCD Research Laboratory, and the clinicians at the McGill University Health Centre for their involvement in this project. J. C. H. and M. D. thank the Université de Sherbrooke Research Chair in Neuroinformatics.

This study was supported by funding from McGill University and the Research Institute of the McGill University Health Centre. At the time of the study, K. E. received studentship support in the form of: a Canada Graduate Scholarship – Master's from the Canadian Institutes of Health Research; funding from the Canada First Research Excellence Fund, awarded to McGill University for the Healthy Brains for Healthy Lives initiative; and a Lasha Research Fellowship from the McGill University Faculty of Medicine.

Abbreviations

AD	axial diffusivity
CHD	congenital heart disease
DTI	diffusion tensor imaging
FA	fractional anistropy
HARDI	high angular resolution diffusion imaging
MD	mean diffusivity
MRI	magnetic resonance imaging
NDI	neurite density index
NODDI	neurite orientation dispersion and density imaging
ODI	orientation dispersion index
preOLs	pre-myelinating late oligodendrocyte progenitors
RD	radial diffusivity
TBSS	tract-based spatial statistics
V_{iso}	isotropic volume fraction

References

Abda, A., Bolduc, M.E., Tsimicalis, A., Rennick, J., Vatcher, D., Brossard-Racine, M., 2019. Psychosocial outcomes of children and adolescents with Severe congenital heart defect: a systematic review and meta-analysis. J. Pediatr. Psychol. 44 (4), 463–477. https://doi.org/10.1093/jpepsy/jsy085.

Back, S.A., Miller, S.P., 2014. Brain injury in premature neonates: a primary cerebral dysmaturation disorder? Ann. Neurol. 75 (4), 469–486. https://doi.org/10.1002/ana.24132.

Bellinger, D.C., Wypij, D., Rivkin, M.J., DeMaso, D.R., Robertson Jr., R.L., Dunbar-Masterson, C., et al., 2011. Adolescents with d-transposition of the great arteries corrected with the arterial switch procedure: neuropsychological assessment and structural brain imaging. Circulation 124 (12), 1361–1369. https://doi.org/10.1161/CIRCULATIONAHA.111.026963.

Benjamini, Y., Hochberg, Y., 1995. Controlling the false discovery rate: a practical and powerful approach to multiple testing. J Royal Stat Soc B 57 (1), 289–300.

Billiet, T., Madler, B., D'Arco, F., Peeters, R., Deprez, S., Plasschaert, E., et al., 2014. Characterizing the microstructural basis of "unidentified bright objects" in neurofibromatosis type 1: a combined in vivo multicomponent T2 relaxation and multi-shell diffusion MRI analysis. Neuroimage Clin 4, 649–658. https://doi.org/10.1016/j.nicl.2014.04.005.

Bolduc, M.E., Lambert, H., Ganeshamoorthy, S., Brossard-Racine, M., 2018. Structural brain abnormalities in adolescents and young adults with congenital heart defect: a

systematic review. Dev. Med. Child Neurol. 60 (12), 1209–1224. https://doi.org/10.1111/dmcn.13975.
Brewster, R.C., King, T.Z., Burns, T.G., Drossner, D.M., Mahle, W.T., 2015. White matter integrity dissociates verbal memory and auditory attention span in emerging adults with congenital heart disease. J. Int. Neuropsychol. Soc. 21 (1), 22–33. https://doi.org/10.1017/S135561771400109X.
Chang, Y.S., Owen, J.P., Pojman, N.J., Thieu, T., Bukshpun, P., Wakahiro, M.L., et al., 2015. White matter changes of neurite density and fiber orientation dispersion during human brain maturation. PLoS One 10 (6), e0123656. https://doi.org/10.1371/journal.pone.0123656.
Cousineau, M., Jodoin, P.M., Morency, F.C., Rozanski, V., Grand'Maison, M., Bedell, B.J., Descoteaux, M., 2017. A test-retest study on Parkinson's PPMI dataset yields statistically significant white matter fascicles. Neuroimage Clin 16, 222–233. https://doi.org/10.1016/j.nicl.2017.07.020.
Daducci, A., Canales-Rodriguez, E.J., Zhang, H., Dyrby, T.B., Alexander, D.C., Thiran, J.P., 2015. Accelerated microstructure imaging via convex optimization (AMICO) from diffusion MRI data. Neuroimage 105, 32–44. https://doi.org/10.1016/j.neuroimage.2014.10.026.
Dell'Acqua, F., Simmons, A., Williams, S.C., Catani, M., 2013. Can spherical deconvolution provide more information than fiber orientations? Hindrance modulated orientational anisotropy, a true-tract specific index to characterize white matter diffusion. Hum. Brain Mapp. 34 (10), 2464–2483. https://doi.org/10.1002/hbm.22080.
Di Tommaso, P., Chatzou, M., Floden, E.W., Barja, P.P., Palumbo, E., Notredame, C., 2017. Nextflow enables reproducible computational workflows. Nat. Biotechnol. 35 (4), 316–319. https://doi.org/10.1038/nbt.3820.
Dimitropoulos, A., McQuillen, P.S., Sethi, V., Moosa, A., Chau, V., Xu, D., et al., 2013. Brain injury and development in newborns with critical congenital heart disease. Neurology 81 (3), 241–248. https://doi.org/10.1212/WNL.0b013e31829bfdcf.
Donofrio, M.T., Bremer, Y.A., Schieken, R.M., Gennings, C., Morton, L.D., Eidem, B.W., et al., 2003. Autoregulation of cerebral blood flow in fetuses with congenital heart disease: the brain sparing effect. Pediatr. Cardiol. 24 (5), 436–443. https://doi.org/10.1007/s00246-002-0404-0.
Easson, K., Dahan-Oliel, N., Rohlicek, C., Sahakian, S., Brossard-Racine, M., Mazer, B., et al., 2019. A comparison of developmental outcomes of adolescent neonatal intensive care unit survivors born with a congenital heart defect or born preterm. J. Pediatr. 207, 34–41. https://doi.org/10.1016/j.jpeds.2018.11.002.
FMRIB Analysis Group, 2012. FMRIB58_FA. https://fsl.fmrib.ox.ac.uk/fsl/fslwiki/FMRIB58_FA (accessed 30 August 2019).
Fontes, K., Rohlicek, C.V., Saint-Martin, C., Gilbert, G., Easson, K., Majnemer, A., et al., 2019. Hippocampal alterations and functional correlates in adolescents and young adults with congenital heart disease. Hum. Brain Mapp. 40 (12), 4548–4560. https://doi.org/10.1002/hbm.24615.
Garyfallidis, E., Cote, M.A., Rheault, F., Sidhu, J., Hau, J., Petit, L., et al., 2018. Recognition of white matter bundles using local and global streamline-based registration and clustering. Neuroimage 170, 283–295. https://doi.org/10.1016/j.neuroimage.2017.07.015.
Genc, S., Malpas, C.B., Holland, S.K., Beare, R., Silk, T.J., 2017. Neurite density index is sensitive to age related differences in the developing brain. Neuroimage 148, 373–380. https://doi.org/10.1016/j.neuroimage.2017.01.023.
Girard, G., Whittingstall, K., Deriche, R., Descoteaux, M., 2014. Towards quantitative connectivity analysis: reducing tractography biases. Neuroimage 98, 266–278. https://doi.org/10.1016/j.neuroimage.2014.04.074.
Heinrichs, A.K., Holschen, A., Krings, T., Messmer, B.J., Schnitker, R., Minkenberg, R., Hovels-Gurich, H.H., 2014. Neurologic and psycho-intellectual outcome related to structural brain imaging in adolescents and young adults after neonatal arterial switch operation for transposition of the great arteries. J. Thorac. Cardiovasc. Surg. 148 (5), 2190–2199. https://doi.org/10.1016/j.jtcvs.2013.10.087.
Hollingshead, A.B., 2011. Four factor index of social status. Yale Journal of Sociology 8, 21–51.
Hua, K., Zhang, J., Wakana, S., Jiang, H., Li, X., Reich, D.S., et al., 2008. Tract probability maps in stereotaxic spaces: analyses of white matter anatomy and tract-specific quantification. Neuroimage 39 (1), 336–347. https://doi.org/10.1016/j.neuroimage.2007.07.053.
Jednorog, K., Altarelli, I., Monzalvo, K., Fluss, J., Dubois, J., Billard, C., et al., 2012. The influence of socioeconomic status on children's brain structure. PLoS One 7 (8), e42486. https://doi.org/10.1371/journal.pone.0042486.
Jeurissen, B., Leemans, A., Tournier, J.D., Jones, D.K., Sijbers, J., 2013. Investigating the prevalence of complex fiber configurations in white matter tissue with diffusion magnetic resonance imaging. Hum. Brain Mapp. 34 (11), 2747–2766. https://doi.org/10.1002/hbm.22099.
Jones, D.K., Knosche, T.R., Turner, R., 2013. White matter integrity, fiber count, and other fallacies: the do's and don'ts of diffusion MRI. Neuroimage 73, 239–254. https://doi.org/10.1016/j.neuroimage.2012.06.081.
Kaden, E., Kruggel, F., Alexander, D.C., 2016. Quantitative mapping of the per-axon diffusion coefficients in brain white matter. Magn. Reson. Med. 75 (4), 1752–1763. https://doi.org/10.1002/mrm.25734.
Karmacharya, S., Gagoski, B., Ning, L., Vyas, R., Cheng, H.H., Soul, J., et al., 2018. Advanced diffusion imaging for assessing normal white matter development in neonates and characterizing aberrant development in congenital heart disease. Neuroimage Clin 19, 360–373. https://doi.org/10.1016/j.nicl.2018.04.032.
Kurtzer, G.M., Sochat, V., Bauer, M.W., 2017. Singularity: scientific containers for mobility of compute. PLoS One 12 (5), e0177459. https://doi.org/10.1371/journal.pone.0177459.
Lampinen, B., Szczepankiewicz, F., Martensson, J., van Westen, D., Sundgren, P.C., Nilsson, M., 2017. Neurite density imaging versus imaging of microscopic anisotropy in diffusion MRI: a model comparison using spherical tensor encoding. Neuroimage 147, 517–531. https://doi.org/10.1016/j.neuroimage.2016.11.053.
Lampinen, B., Szczepankiewicz, F., Noven, M., van Westen, D., Hansson, O., Englund, E., et al., 2019. Searching for the neurite density with diffusion MRI: challenges for biophysical modeling. Hum. Brain Mapp. 40 (8), 2529–2545. https://doi.org/10.1002/hbm.24542.
Latal, B., 2016. Neurodevelopmental outcomes of the child with congenital heart disease. Clin. Perinatol. 43 (1), 173–185. https://doi.org/10.1016/j.clp.2015.11.012.
Lebel, C., Beaulieu, C., 2011. Longitudinal development of human brain wiring continues from childhood into adulthood. J. Neurosci. 31 (30), 10937–10947. https://doi.org/10.1523/JNEUROSCI.5302-10.2011.
Mah, A., Geeraert, B., Lebel, C., 2017. Detailing neuroanatomical development in late childhood and early adolescence using NODDI. PLoS One 12 (8), e0182340. https://doi.org/10.1371/journal.pone.0182340.
Makris, N., Kennedy, D.N., McInerney, S., Sorensen, A.G., Wang, R., Caviness Jr., V.S., Pandya, D.N., 2005. Segmentation of subcomponents within the superior longitudinal fascicle in humans: a quantitative, in vivo, DT-MRI study. Cerebr. Cortex 15 (6), 854–869. https://doi.org/10.1093/cercor/bhh186.
Marelli, A., Miller, S.P., Marino, B.S., Jefferson, A.L., Newburger, J.W., 2016. Brain in congenital heart disease across the lifespan: the cumulative burden of injury. Circulation 133 (20), 1951–1962. https://doi.org/10.1161/CIRCULATIONAHA.115.019881.
McQuillen, P.S., Barkovich, A.J., Hamrick, S.E., Perez, M., Ward, P., Glidden, D.V., et al., 2007. Temporal and anatomic risk profile of brain injury with neonatal repair of congenital heart defects. Stroke 38 (2 Suppl. l), 736–741. https://doi.org/10.1161/01.STR.0000247941.41234.90.
Miller, S.P., McQuillen, P.S., Vigneron, D.B., Glidden, D.V., Barkovich, A.J., Ferriero, D.M., et al., 2004. Preoperative brain injury in newborns with transposition of the great arteries. Ann. Thorac. Surg. 77 (5), 1698–1706. https://doi.org/10.1016/j.athoracsur.2003.10.084.
Miller, S.P., Ferriero, D.M., Leonard, C., Piecuch, R., Glidden, D.V., Partridge, J.C., et al., 2005. Early brain injury in premature newborns detected with magnetic resonance imaging is associated with adverse early neurodevelopmental outcome. J. Pediatr. 147 (5), 609–616. https://doi.org/10.1016/j.jpeds.2005.06.033.
Mori, S., Wakana, S., van Zijl, P., 2005. MRI Atlas of Human White Matter. Elsevier, Amsterdam.
Morton, P.D., Ishibashi, N., Jonas, R.A., 2017. Neurodevelopmental abnormalities and congenital heart disease: insights into altered brain maturation. Circ. Res. 120 (6), 960–977. https://doi.org/10.1161/CIRCRESAHA.116.309048.
Nave, K.A., 2010. Myelination and support of axonal integrity by glia. Nature 468 (7321), 244–252. https://doi.org/10.1038/nature09614.
Nichols, T.E., Holmes, A.P., 2002. Nonparametric permutation tests for functional neuroimaging: a primer with examples. Hum. Brain Mapp. 15 (1), 1–25.
Noble, K.G., Houston, S.M., Kan, E., Sowell, E.R., 2012. Neural correlates of socioeconomic status in the developing human brain. Dev. Sci. 15 (4), 516–527. https://doi.org/10.1111/j.1467-7687.2012.01147.x.
Owen, M., Shevell, M., Majnemer, A., Limperopoulos, C., 2011. Abnormal brain structure and function in newborns with complex congenital heart defects before open heart surgery: a review of the evidence. J. Child Neurol. 26 (6), 743–755. https://doi.org/10.1177/0883073811402073.
Peyvandi, S., De Santiago, V., Chakkarapani, E., Chau, V., Campbell, A., Poskitt, K.J., et al., 2016. Association of prenatal diagnosis of critical congenital heart disease with postnatal brain development and the risk of brain injury. JAMA Pediatr 170 (4), e154450. https://doi.org/10.1001/jamapediatrics.2015.4450.
Raffelt, D., Tournier, J.D., Rose, S., Ridgway, G.R., Henderson, R., Crozier, S., et al., 2012. Apparent Fibre Density: a novel measure for the analysis of diffusion-weighted magnetic resonance images. Neuroimage 59 (4), 3976–3994. https://doi.org/10.1016/j.neuroimage.2011.10.045.
Rivkin, M.J., Watson, C.G., Scoppettuolo, L.A., Wypij, D., Vajapeyam, S., Bellinger, D.C., et al., 2013. Adolescents with D-transposition of the great arteries repaired in early infancy demonstrate reduced white matter microstructure associated with clinical risk factors. J. Thorac. Cardiovasc. Surg. 146 (3), 543–549. https://doi.org/10.1016/j.jtcvs.2012.12.006 e541.
Schmahmann, J.D., Smith, E.E., Eichler, F.S., Filley, C.M., 2008. Cerebral white matter: neuroanatomy, clinical neurology, and neurobehavioral correlates. Ann. N. Y. Acad. Sci. 1142, 266–309. https://doi.org/10.1196/annals.1444.017.
Simons, M., Nave, K.A., 2015. Oligodendrocytes: myelination and axonal support. Cold Spring Harb Perspect Biol 8 (1), a020479. https://doi.org/10.1101/cshperspect.a020479.
Smith, S.M., Nichols, T.E., 2009. Threshold-free cluster enhancement: addressing problems of smoothing, threshold dependence and localisation in cluster inference. Neuroimage 44 (1), 83–98. https://doi.org/10.1016/j.neuroimage.2008.03.061.
Smith, S.M., Jenkinson, M., Woolrich, M.W., Beckmann, C.F., Behrens, T.E., Johansen-Berg, H., et al., 2004. Advances in functional and structural MR image analysis and implementation as FSL. Neuroimage 23 (Suppl. 1), S208–S219. https://doi.org/10.1016/j.neuroimage.2004.07.051.
Smith, S.M., Jenkinson, M., Johansen-Berg, H., Rueckert, D., Nichols, T.E., Mackay, C.E., et al., 2006. Tract-based spatial statistics: voxelwise analysis of multi-subject diffusion data. Neuroimage 31 (4), 1487–1505. https://doi.org/10.1016/j.neuroimage.2006.02.024.
Sun, L., Macgowan, C.K., Sled, J.G., Yoo, S.J., Manlhiot, C., Porayette, P., et al., 2015. Reduced fetal cerebral oxygen consumption is associated with smaller brain size in fetuses with congenital heart disease. Circulation 131 (15), 1313–1323. https://doi.org/10.1161/CIRCULATIONAHA.114.013051.

Theaud, G., Houde, J.C., Boré, A., Rheault, F., Morency, F., Descoteaux, M., 2019. TractoFlow: A Robust, Efficient and Reproducible Diffusion MRI Pipeline Leveraging Nextflow & Singularity bioRxiv, 631952.

Tournier, J.D., Calamante, F., Connelly, A., 2007. Robust determination of the fibre orientation distribution in diffusion MRI: non-negativity constrained super-resolved spherical deconvolution. Neuroimage 35 (4), 1459–1472. https://doi.org/10.1016/j.neuroimage.2007.02.016.

Tustison, N.J., Avants, B.B., Cook, P.A., Zheng, Y., Egan, A., Yushkevich, P.A., Gee, J.C., 2010. N4ITK: improved N3 bias correction. IEEE Trans. Med. Imaging 29 (6), 1310–1320. https://doi.org/10.1109/TMI.2010.2046908.

Ursache, A., Noble, K.G., Pediatric Imaging, N., Genetics, S., 2016. Socioeconomic status, white matter, and executive function in children. Brain Behav 6 (10), e00531. https://doi.org/10.1002/brb3.531.

Veraart, J., Novikov, D.S., Christiaens, D., Ades-Aron, B., Sijbers, J., Fieremans, E., 2016. Denoising of diffusion MRI using random matrix theory. Neuroimage 142, 394–406. https://doi.org/10.1016/j.neuroimage.2016.08.016.

von Rhein, M., Scheer, I., Loenneker, T., Huber, R., Knirsch, W., Latal, B., 2011. Structural brain lesions in adolescents with congenital heart disease. J. Pediatr. 158 (6), 984–989. https://doi.org/10.1016/j.jpeds.2010.11.040.

von Rhein, M., Buchmann, A., Hagmann, C., Huber, R., Klaver, P., Knirsch, W., Latal, B., 2014. Brain volumes predict neurodevelopment in adolescents after surgery for congenital heart disease. Brain 137 (Pt 1), 268–276. https://doi.org/10.1093/brain/awt322.

Wakana, S., Caprihan, A., Panzenboeck, M.M., Fallon, J.H., Perry, M., Gollub, R.L., et al., 2007. Reproducibility of quantitative tractography methods applied to cerebral white matter. Neuroimage 36 (3), 630–644. https://doi.org/10.1016/j.neuroimage.2007.02.049.

Watson, C.G., Stopp, C., Wypij, D., Bellinger, D.C., Newburger, J.W., Rivkin, M.J., 2018. Altered white matter microstructure correlates with IQ and processing speed in children and adolescents post-fontan. J. Pediatr. 200, 140–149 e144. https://doi.org/10.1016/j.jpeds.2018.04.022.

Zhang, J., Evans, A., Hermoye, L., Lee, S.K., Wakana, S., Zhang, W., et al., 2007. Evidence of slow maturation of the superior longitudinal fasciculus in early childhood by diffusion tensor imaging. Neuroimage 38 (2), 239–247. https://doi.org/10.1016/j.neuroimage.2007.07.033.

Zhang, H., Schneider, T., Wheeler-Kingshott, C.A., Alexander, D.C., 2012. NODDI: practical in vivo neurite orientation dispersion and density imaging of the human brain. Neuroimage 61 (4), 1000–1016. https://doi.org/10.1016/j.neuroimage.2012.03.072.

Zucchelli, M., Descoteaux, M., Menegaz, G., 2017. NODDI-SH: a Computational Efficient NODDI Extension for fODF Estimation in Diffusion MRI arXiv preprint arXiv: 1708.08999.